Molecular Genetics & Genomic Medicine
Open Access **WILEY**

ECEL1 novel mutation in arthrogryposis type 5D: A molecular dynamic simulation study

Najmeh Ahangari[1,2] | **Nazanin Gholampour-Faroji**[3] | **Mohammad Doosti**[2] |
Majid Ghayour Mobarhan[4] ⬤ | **Sima Shahrokhzadeh**[2] | **Ehsan Ghayoor Karimiani**[2,5,6] |
Bahareh Hasani-sabzevar[7] | **Paria Najarzadeh Torbati**[2] ⬤ |
Aliakbar Haddad-Mashadrizeh[8]

[1]Innovative Medical Research Center, Faculty of Medicine, Mashhad Medical Science, Islamic Azad University, Mashhad, Iran

[2]Department of Medical Genetics, Next Generation Genetic Polyclinic, Mashhad, Iran

[3]Biotechnology Department, Iranian Research Organization for Science and Technology (IROST), Tehran, Iran

[4]Metabolic Syndrome Research Center, School of Medicine, Mashhad University of Medical Sciences, Mashhad, Iran

[5]Molecular and Clinical Sciences Institute, St. George's University of London, Cranmer Terrace, London, UK

[6]Department of Molecular Genetics, Next Generation Genetic Polyclinic, Mashhad, Iran

[7]Advanced computational center, Khayyam Innovation Ecosystem, Mashhad, Iran

[8]Industrial Biotechnology Research Group, Institute of Biotechnology, Ferdowsi University of Mashhad, Mashhad, Iran

Correspondence
Ehsan Ghayoor Karimiani, Molecular, and Clinical Sciences Institute, St. George's University of London, Cranmer Terrace, London SW17 0RE, UK. Department of Molecular Genetics, Next Generation Genetic Polyclinic, Mashhad 009851, Iran.
Email: eghayoor@gmail.com

Aliakbar Haddad-Mashadrizeh, Industrial Biotechnology Research Group, Institute of Biotechnology, Ferdowsi University of Mashhad, Mashhad, Iran.
Email: a.haddad@um.ac.ir

Abstract

Background: *ECEL1* has been presented as a causal gene of an autosomal recessive form distal arthrogryposis (DA) which affects the distal joints. The present study focused on bioinformatic analysis of a novel mutation in *ECEL1*, c.535A>G (p. Lys179Glu), which was reported in a family with 2 affected boys and fetus through prenatal diagnosis.

Methods: Whole-exome sequencing data analyzed followed by molecular dynamic (MD) simulation of native ECEL1 protein and mutant structures using GROMACS software. One variant c.535A>G, p. Lys179Glu (homozygous) on gene *ECEL1* has been detected in proband which was validated in all family members through Sanger sequencing.

Results: We demonstrated remarkable constructional differences by MD simulation between wild-type and novel mutant of *ECEL1* gene. The reason for the lack of the Zn ion binding in mutation in the ECEL1 protein has been identified by average atomic distance and SMD analysis among the wild-type and mutant.

Conclusion: Overall, in this study, we present knowledge of the effect of the studied variant on the ECEL1 protein leading to neurodegenerative disorder in humans. This work may hopefully be supplementary to classical molecular dynamics to dissolve the mutational effects of cofactor-dependent protein.

1 | INTRODUCTION

Distal arthrogryposis syndromes (DAs) demonstrate a wide clinical variability and similar clinical findings with the other arthrogryposis types which were classified previously. Most of the das are inherited as autosomal dominant disorders. DA type 5D is a subtype of DA type 5 inherited as an autosomal recessive disorder, clinically characterized by congenital distal joint contractures, knee extension contractures, congenital hip dislocation, club foot, ptosis, and other eye findings, furrowed tongue, and scoliosis. Arthrogryposis shows congenital contracture in at least two different body parts. The term distal arthrogryposis (DA) is used when distal joints are primarily involved. Assessment of distinct clinical subtypes of DA has proven very useful in finding the disease-causing genetic variants for this genetically heterogenous condition (Patil et al., 2014; Shaheen et al., 2014).

ECEL1 encodes endothelin-converting enzyme-like 1 (*ECEL1*; OMIM: 605896) also known as damage-induced neuronal endopeptidase, is a membrane-bound metalloprotease that does not cleave ECE substrates although its structural similarity to the endothelin-converting enzyme (ECE) (Shirotani et al., 2001). By analyzing candidate genes in a critical region of 2q identified in a family with autosomal recessive distal arthrogryposis, as well as in 2 additional families with a similar recessive DA phenotype, Mcmillin et al. (2013) identified homozygously or compound heterozygous variants in only a single gene, *ECEL1* (Li et al., 2015). The *ECEL1* gene encodes a member of the M13 family of endopeptidases. Members of this family are zinc-containing type II integral-membrane proteins that are important regulators of neuropeptide and peptide hormone activity [provided by Refseq, Mar 2014]. Chromosomal Location is 2q37.1 (Homo sapiens Annotation Release 108, grch38.p7) (NCBI) and consists of 18 exons which encode 775 amino acids, an 87791KD protein. It has been shown that the *ECEL1* gene is expressed in the CNS, in particular in the putamen, spinal cord, medulla, and subthalamic nucleus. Data demonstrated lower levels of *ECEL1* expression in the amygdala, caudate, thalamus, pancreas, and skeletal muscle; and very low levels in the substantia nigra, cerebellum, cortex, corpus callosum, and hippocampus. Since the *ECEL1* gene is predominantly expressed in neuronal cells, suggesting unique neurogenic pathogenesis in a subset of DA patients with *ECEL1* mutation. The present study focused on the analysis of a novel mutation in *ECEL1*, c.535A>G (p. Lys179Glu), which was reported in a family with 2 affected boys and a fetus through prenatal diagnosis. This article aimed to describe the main aspects of this gene and predicting the efficacy of this mutation on ECEL1 protein characteristics and function.

2 | MATERIALS AND METHODS

2.1 | Editorial policies and ethical considerations

All procedures performed in studies involving human participants were by the ethical standards of the institutional research committee and with the 1964 Helsinki declaration and its later amendments or comparable ethical standards.

2.2 | Case presentation

The family was referred by a neurologist and gynecologist for genetic counseling during pregnancy and probable prenatal diagnosis. The parents were first cousins and the mother was pregnant (6 weeks). Proband II.2 was a 12-year-old boy, and his younger brother, proband II.3, was 8 years old. The clinical manifestations of the affected children are as follows: mild ptosis and limitation of ocular motility in the vertical direction, decreased facial movements, speech difficulties, limited shoulder movement, limited elbow movement, severe contracture of fingers II-V, talus valgus, deformity of feet and difficulty in walking.

According to the clinical history, the medical geneticist explained the situation to the family. After obtaining their written informed consent, blood samples were collected from all family members including parents and patients. DNA extraction was done using QIAGEN mini kit according to the manufacturer's instructions and processed for whole-exome sequencing (WES 200X Macrogen, Korea) in one patient, proband II.2. After obtaining the WES result and data analysis, the reads were aligned to the human reference genome (grch37.1/hg19). Only variants located in coding regions were picked up. Common variants were excluded. To investigate candidate variants in other family members, specific primers were designed. During the molecular genetic analysis, a fetal anomaly scan at 18 weeks of pregnancy, revealed skeletal dysplasia in the fetus. Amniocentesis was done and fetal DNA was extracted using QIAGEN mini kit. The candidate variant was sequenced in

parents, proband II.3, and fetus with an ABI PRISM 3130xl Genetic Analyzer (Life Technologies Inc., Carlsbad, CA) and analyzed using FinchTV software version 1.4.0.

Since the pedigree showed an autosomal recessive pattern, we sequenced all family members. One variant c.535A>G, p. Lys179Glu (homozygous) on gene *ECEL1* has been detected in both affected individuals. Both parents were heterozygous for this variant. The result revealed that unfortunately, the fetus was mutated homozygous as well. Bioinformatics analysis of this variant showed a destructive effect on the protein. The homozygous variant c.535A>G, p. Lys179Glu on gene *ECEL1* is conclusive that this gene is pathogenic for the diagnosis of distal arthrogryposis syndromes (DAs) type 5D. The family pedigree, clinical manifestation, and sequencing results are shown in Figure 1.
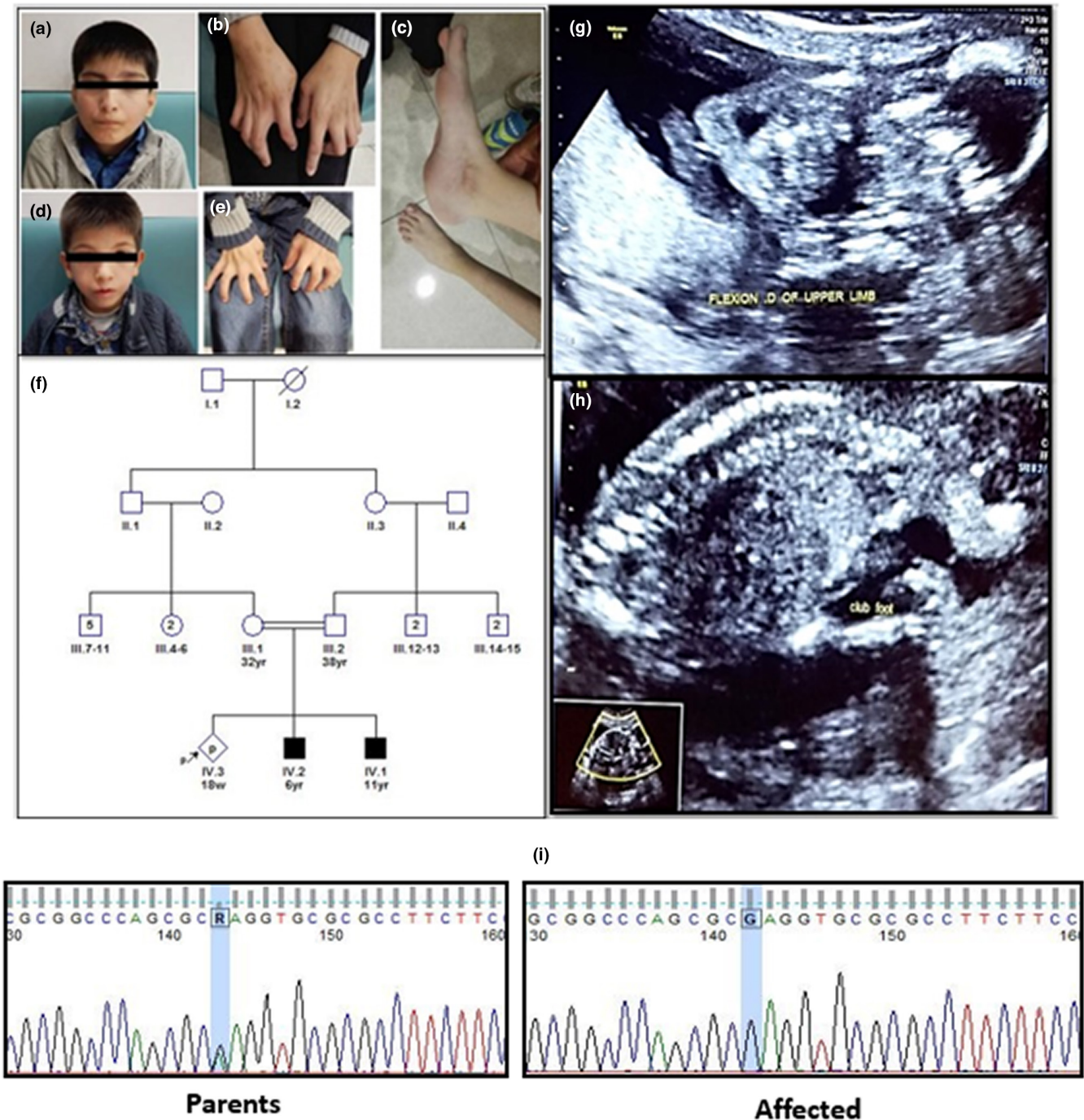

FIGURE 1 (a–e) Typical features of arthrogryposis including a small jaw, flexed fingers II-V, talus valgus and deformity of feet, (f) pedigree showing the relationships and affected status of family, (g) ultra scan image of fetus shows flexion of upper limb, (h) club feet, (i) sequencing results for fetus and parents showed c.535A>G mutation in exon2 of *ECEL1* gene.

2.3 | Sequence and structure data

The human *ECEL1* DNA sequence in FASTA format was retrieved from NCBI Gene (Accession number NG_034065.1). It is located on chromosome 2q37.1, contains 18 exons and spans approximately 8 Kb (2:232,479,826-232,487,858). This gene has 4 transcripts which encode 775aa, 773aa, 168aa, respectively. The 4th transcript translates no protein. The human ECEL1 protein sequence (O95672) was obtained from the UNIPROT database.

2.4 | Selection of variants for in silico analysis

As shown in Figure 2a, ClinVar was used to retrieve pathogenic variants reported for the *ECEL1* gene (https://www.ncbi.nlm.nih.gov/clinvar).

2.5 | Mutation functionality prediction

Subsequently, the effect of mutation (K179E) on *ECEL1* protein function was analyzed with the best prediction tools (MutPred, FATHMM-MKL, SIFT, PROVEAN, and Mutation Taster), for exact predictions with the prediction score (Table 1).

2.6 | Modeling of the ECEL1 protein structure and mutations

It is crucial to obtain the 3D structure of the protein to study its function, particularly to realize the efficacy of SNPs on its structure and function in general. We used the SWISS Model online server for modeling the crystal structures of the wild-type of human ECEL1 protein. (https://swissmodel.expasy.org/). We used the "mutagenesis" tool for performing the modeling of the mutated protein structures in the PyMOL Molecular Graphics System v.1.3 (Schrodinger, LLC) using the 3D structure of wild-type modeled.

2.7 | Model validation

For validation, the quality of the models was assessed by ProSA-web (https://prosa.services.came.sbg.ac.at/prosa.php).
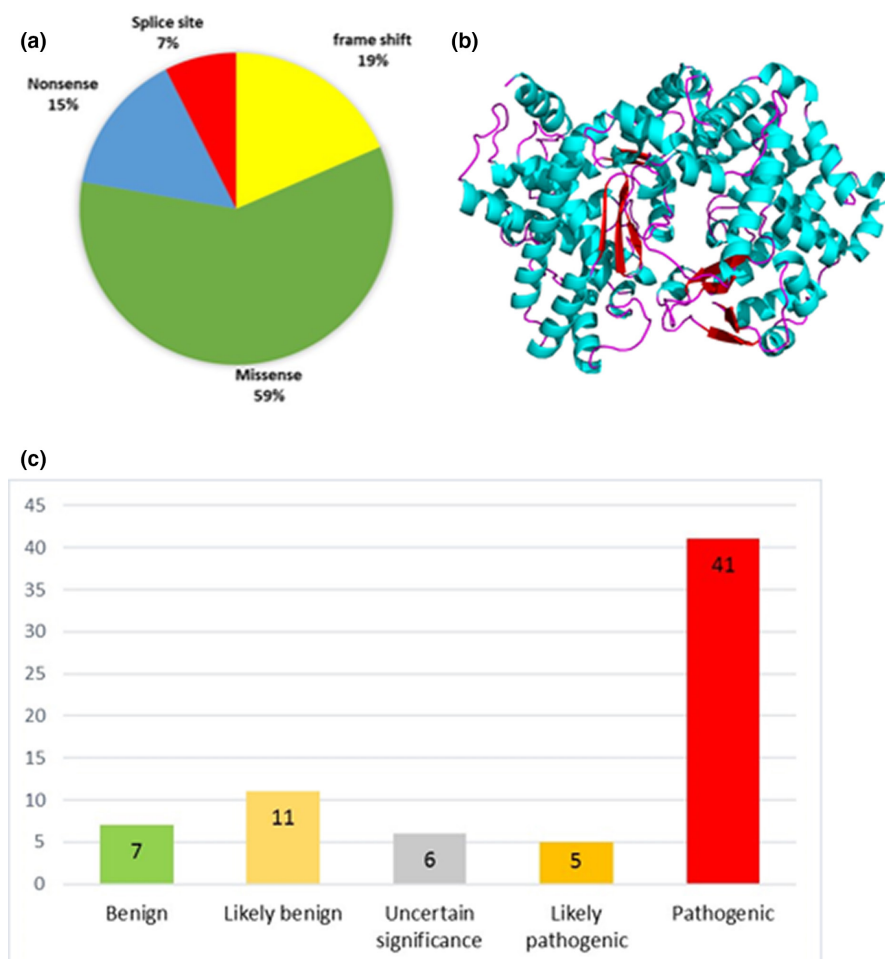
FIGURE 2 (a) Clinical significance of *ECEL1* gene variants reported in Clin Var database based on the ACMG classification, (b) normal structure of ECEL1 protein (O95672). Model from amino acids 102–775. (c) Frequency of *ECEL1* gene variants based on the molecular consequence.

TABLE 1 Prediction results using the most helpful online prediction tools for K179E.

Prediction tool	Prediction	URL
Mutpred	Pathogenic	Http://mutpred.mutdb.org/
FATHMM-MKL	Damaging	Http://fathmm.biocompute.org.uk/fathmmmkl.htm
SIFT	Damaging	Https://sift.bii.a-star.edu.sg/www/SIFT_seq_submit2.html
PROVEAN	Damaging	Http://provean.jcvi.org/index.php
Mutationtaster	Disease-causing	Http://www.mutationtaster.org/

Next, to further validate, the modeled structure was assessed by ERRAT, Verify3D, and Ramachandran plot in PROCHECK as previously described (Colovos & Yeates, 1993; Eisenberg et al., 1997; Gholampour-Faroji et al., 2019; Laskowski et al., 1993).

2.8 | Molecular dynamics simulations

To compare the structural changes with time, we performed molecular dynamic (MD) simulation of native ECEL1 protein and mutant structures using GROMACS version 5.0.7. The force field used was GROMOS96 43a1. In a cubic cell filled with ingle point charged (SPC/E) water, the 3D structures were placed and box set at 1.0 nm (nm). Sodium or chloride ions were added for neutralizing the total charge of the system. Position constraints were applied to proteins and heavy atoms, and simulations were used for the NVT equilibrium group in which the number of particles is present, using the velocity rescaling method, the temperature and the volume of the system were preserved constantly at 310.15 K for 100 ps (Hess et al., 1997). Using Nose-Hoover thermostat and Parrinello-Rahman barostat, the temperature and pressure were controlled. After the system's well-equilibration, we ran a 10 ns (nanoseconds) of MD simulation for our protein structure prediction and all mutants. We used the linear constraint solver (LINCS) algorithm for constraining all bonds by using a 2 fs (femtoseconds) time-step (Hess et al., 1997). As mentioned before, the consistency and conformational changes in the ECEL1 protein and the mutant variants were evaluated by the analysis of root-mean-square deviation (RMSD), root-mean-square fluctuation (RMSF), radius of gyration (Rg), and number of hydrogen bonds (Hb) (Valdenaire et al., 2000). We used the excel tool for creating all graphs.

2.9 | Statistical calculations

A prominent assessment along with experimental studies is provided by statistical dynamic analysis (Whyte et al., 2014). Thus, in this study, the accuracy and precision of the statistical results came by the path of accomplishing

the wild-type and mutant variant in the ECEL1 gene. For statistically investigating, we performed a non-parametric Wilcoxon rank-sum test using excel for the RMSD, RMSF, Rg, and the Zn-binding residues distance differences. Manifesting the results of trajectory analysis, as well as the possibility of prediction between the wild-type and mutant ECEL1, provided by the p-value, acquired from the Wilcoxon method.

3 | RESULTS AND DISCUSSION

A single amino acid changing in protein may alter the protein folding, constancy, and biochemical functions leading to negative effects. (Pires et al., 2016). The efficacy of a point mutation at K179E in the ECEL1 gene which causes the Distal Arthrogryposis type 5D has been indicated in this study. In addition, it is elucidated how the deflection in spatial arrangements of wild-type and mutation of ECEL1 changes their conformations.

3.1 | Mutation functionality prediction

We first evaluated the sequence of ECEL1 obtained from the UNIPROT database in Polyphen2, Mutation Taster, SIFT, and PhD-SNP. We performed substitution amino acid at K179E and for prediction. Consequently, the programs predicted the analysis from these different tools. The results from all tools predicted that the mutation is damaging. All the assurance scores obtained from tools are gathered in Table 1. These first results demonstrated that the mutation has a deleterious effect on ECEL1 protein function. The effects of mutant variants on protein are revealed in this way, leading to the next level of comprehension about its influence on ECEL1.

3.2 | Structural modeling and 3D structure validation

The three-dimensional structure of the ECEL1 protein (Figure 2b) was generated with the method of the

homology modeling through the Swiss model server using PDB ID: 3dwb as a template and the sequence identity score was 39.31%. For specifying which modeled structure should be used in the next levels, we assessed the modeled structures by the validation algorithms PROCHECK, Rampage, Verify3D, ERRAT, and prose. Phi(F) and psi(ψ) twisting angles for all residues of the protein are shown in the Ramachandran plots acquired from PROCHECK and Rampage, these algorithms evaluate the total quality of stereochemical of a protein structure. It is demonstrated from PROCHECK's Ramachandran plot that, 90.0% of residues lie in most favored regions, 9.3% in additional allowed regions,

0.3% in generously allowed regions, and 0.3% in disallowed regions (Figure 3c).

We used Verify3D, an algorithm that compares the 3D model to its one-dimensional aminoacid sequence for analysis of the exactitude of the tridimensional model, for confirmation of the quality of the final model; the good quality was confirmed, as 91.70% of the residues showed a 3D-1D score higher than 0.2. Then it shows 90.06 overall quality factor for the ultimate model by ERRAT plot and because of the scores being higher than 50, more supportive of its good quality is considered acceptable (Figure 3a). We performed by the prosa web algorithm another alike analysis according to the final structure and obtained a
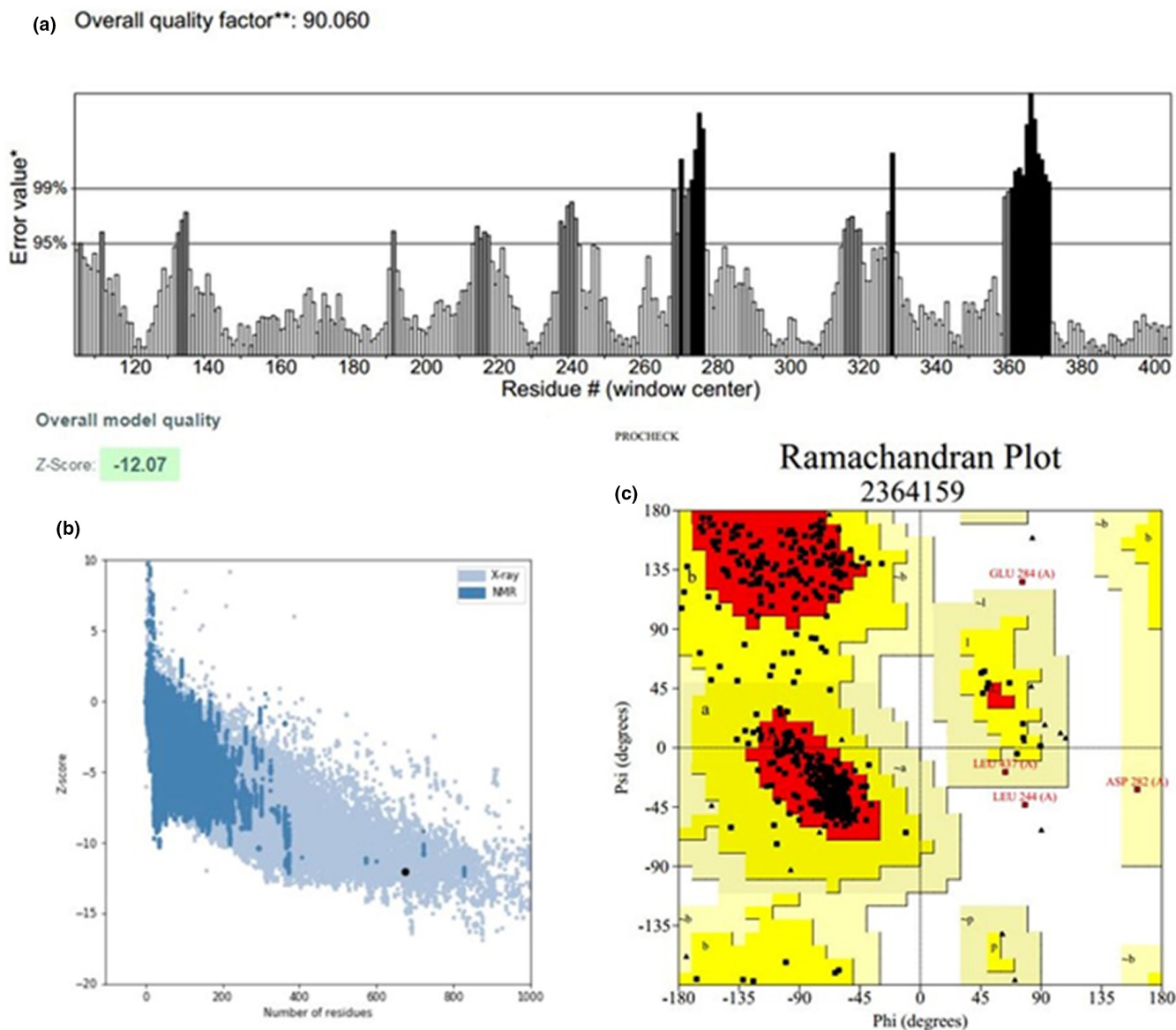

FIGURE 3 Validation of the in silico modeled ECEL1 structure. (a) According to ERRAT plot, the overall quality score that the structure had obtained is 90.06. we used PROCHECK and ERRAT for validating of modeled structure. (b) It is demonstrated that 90.0% of residues lie in most favored regions, 9.3% in additional allowed regions, 0.3% in generously allowed regions and 0.3% in disallowed regions according to PROCHECK's Ramachandran plot (c) Ramachandran Plot.

Z-score of −12.07, and thus, these scores lie in the range of scores that are found on similarly sized proteins, with an X-ray quality (Figure 3b).

3.3 | Analysis of MD simulations

10 nm molecular dynamic simulations were performed for each protein for the comprehension of the structural differences in the protein based on the comparative mutations. Various parameters were analyzed throughout the simulation path, in particular root mean square deviation (RMSD), root mean square fluctuations (RMSF), the whole number of intramolecular hydrogen bonds, and radius of gyration. All important statistical values of the simulation's outcomes are summarized in Table 2. In the present study, the chemical time scale used is sufficient to re-market the side chain in the natural protein state and to facilitate various conformations. Other recent studies demonstrated that a single protein molecule has self-similar dynamic motions, all movements seem similar whether you look at them for picoseconds or 1000s of seconds (Nagata et al., 2017).

To realize the structural changes and the effects of mutations on the protein structure, the RMSD for the backbones of all proteins was calculated during the simulations. As shown in Figure 4a, RMSD values indicate that the mutation structures are completely unstable compared to wild-type proteins. Wild-type protein with an RMSD of about 0.28 nm was stabilized, while most RMSD values of mutant proteins were higher than wild-type, and this figure clearly shows the significant instability effects of the mutations on the protein

structure. Among all mutations, the wild-type R395Q mutant showed the lowest RMSD value and the highest stability, stabilizing at RMSD at about 0.27 nm. Mutant D142E, K179E, G197D, Y290C, R404C, R418S, E423Q, and A675T variants have the highest amount of RMSD compared to the wild-type and other mutants. RMSD for W403C and K179E variants in specific points are much higher and about 0.37. Because of determining the efficacy of mutations on the dynamic behavior of residues of the protein, the RMSF fluctuations of each residue were investigated.

Figure 4b shows that the residual surface fluctuations for E423Q and R404C were quite high compared to natural proteins and other mutants, greater than 0.58 nm for residues at positions 281 and 702, respectively. However, the next highest peak was beheld at approximately the remaining 102 positions for the E423Q with an RMSF of 0.54 nm. Fluctuation analysis showed that the highest degree of flexibility was demonstrated by the mutant protein E423Q.

According to Figure 4c, the radius analysis of wild-type protein was performed with related mutations and compared with each other. When reviewing the statistical data from Table 2, it is inferred that the W403C and K179E mutations have the highest gyrus radius of 2.645 and 2.617 nm, respectively, and the lowest structural compaction. However, mutations R404C and Y290C show the lowest values of gyration radius equal to 2.571 and 2.579 with the highest compaction of the structure. Radiation analysis data show that all mutations cause structural instability effects that result in loss of protein compression, except for D142E, Y290C, R404C, R418S, R418C, and D620N, which have a radius equal to the native protein.

TABLE 2 Analysis of MD trajectory of wild-type and mutated ECEL1 proteins.

| Protein Variant	RMSD Range	Mean	Radius of gyration Range	Mean	Intramolecular H-bonds Range	Mean
WT	0–0.304	0.258	2.573–2.662	2.598	310–363	337.706
D142E	0–0.333	0.296	2.558–2.663	2.589	320–369	346.384
K179E	0–0.385	0.291	2.585–2.659	2.617	320–365	342.762
G197D	0–0.349	0.290	2.5459–2.664	2.591	327–374	352.33
Y290C	0–0.377	0.3062	2.550–2.665	2.579	316–363	341.987
R395Q	0–0.311	0.258	2.567–2.664	2.593	318–365	339.588
W403C	0–0.390	0.315	2.588–2.699	2.645	314–367	337.355
R404C	0–0.341	0.283	2.535–2.659	2.571	310–361	336.92
R418S	0–0.333	0.287	2.5483–2.665	2.589	322–370	348.503
R418C	0–0.302	0.266	2.554–2.658	2.586	311–366	336.745
E423Q	0–0.350	0.294	2.564–2.665	2.595	316–364	340.294
D620N	0–0.334	0.279	2.560–2.658	2.587	327–370	346.768
A675T	0–0.389	0.312	2.579–2.662	2.608	317–365	344.344
C760R	0–0.325	0.275	2.569–2.665	2.605	317–372	346.575
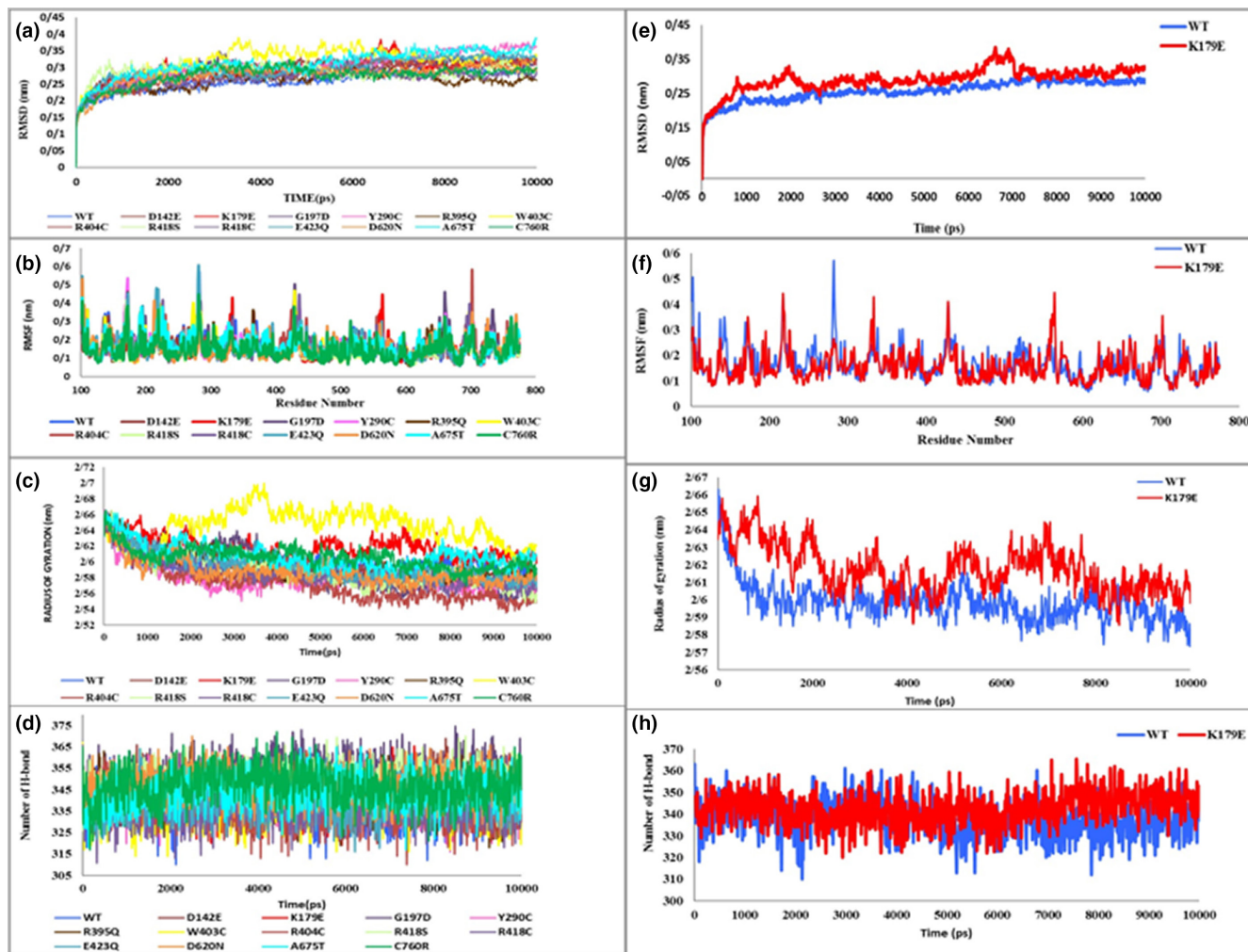
FIGURE 4 (a) RMSD diagram and changes in the structural properties of the ECEL1 protein and the effects of mutations on it. (b) RMSF diagram of ECEL1 protein backbone atoms and mutants. (c) Radius of gyration of ECEL1 protein and its mutants. (d) Total number of intramolecular hydrogen bonds for ECEL1 protein and its mutants. (e) RMSD of the Cα backbone of WT and K179E for 10 ns time period at 310.15 K. (f) The RMSF value for WT and K179E for 10 ns time period at 310.15 K. (g) The radius of gyration compared with time for WT and K179E at 310.15 K. (h) The number of intra-molecular hydrogen bonds for WT and K179E at 310.15 K.

For evaluating the stability of wild-type protein and reported mutations, the total number of intramolecular hydrogen bonds were analyzed according to Figure 4d. As shown in Table 2, the highest number of intramolecular hydrogen bonds was 352.33 for the G197D mutation and 348.503 for the R418S. The number of intramolecular hydrogen bonds for wild-type protein was 337,706. While the lowest number of intramolecular hydrogen bonds was observed for R404C, W403C, R395Q, E423Q, Y290C, K179E, and A675T mutations, respectively, these results suggest that these mutations may destroy the ability to form hydrogen bonds.

To predict protein stability, RMSD was calculated. Figure 4e demonstrates that the total RMSD pattern has changed due to the mutation and its value in the mutation structure has increased. The average RMSD for wild-type and K179E is 0.258 and 0.291, respectively. The RMSD result showed that the K179E mutation was more unstable

than the wild-type protein. From 6 to 7 nanoseconds, the K179E mutation achieved the highest RMSD value of about 0.3 nanometers. The wild-type structure has a fixed pattern and does not oscillate within 10 nanoseconds of the simulation. It is a reputable reality that an appropriate structure is needed for protein activity. Therefore, the RMSD result suggests that the mutant becomes more flexible and changes the geometry of the protein so that the protein cannot perform its normal function.

The RMSF describes the fluctuations of each residual. As shown if Figure 4f, to determine the effect of mutations on the dynamic behavior of residues at the atomic level and to predict structural flexibility after mutation, the RMSF values of the native protein and K179E mutation were analyzed. RMSF values for wild-type were between 0.057 nm to 0.571 nm, and the mean RMSF was 0.165. The RMSF values for the K179E ranged from 0.066 nm to

0.447 nm, and the mean RMSF was 0.154. Fluctuations with RMSF greater than 0.4 nm in the K179E mutation are greater than in the wild-type.

The radius of gravity of a protein is a measure of its density and compaction and shows the extent to which the total distance of the protein atoms from the center of mass of the protein fluctuates. Gyros analysis provides comprehensive information for studying the overall dimensions of the protein. During protein folding, the amount of germination remains constant, but during the protein unfolding process, its amount changes over time. The graph of the radius of gravity for the alpha carbon atoms (according to time) of the native protein and the K179E mutation at 310.15 Kelvin is shown in Figure 4g. The structures of wild-type and K179E mutants showed a radius of gyration ranging from 2.57 to 2.66 nm and 2.58 to 2.65. The average gyrating radius was 2.59 nm for wild-type while it was 2.61 for K179E, indicating that the compact structure of the K179E mutant is lower than that of wild-type. As shown in Figure 4h, the range of intramolecular hydrogen bonds was between 310–363 for wild-type and between 320–365 for K179E. The average number of intramolecular hydrogen bonds for wild-type was 337,706 while for the K179E mutation it was 342,762.

4 | CONCLUSION

This study offers clinical and molecular evidence that mutations in endothelin-converting enzyme-like 1 (*ECEL1*) described arthrogryposis type 5D and its autosomal recessive inheritance with detectable clinical features. *ECEL1* gene is located at q36- q37 region of chromosome 2 and demonstrates to include 18 exons spanning almost 8 kb (Valdenaire et al., 2000). Recently it is found that *ECEL1* has a key role in DA5D. An unknown substrate and transmembrane M13 metallopeptidase type 2 localized to the plasma membrane of the central nervous system (CNS) and endoplasmic reticulum encodes by *ECEL1* (Whyte et al., 2014). The novel mutation c.535A>G alters Lysine (positively charged, a basic amino acid) in position 179 to Glutamate (negatively charged, acidic amino acid). According to bioinformatics analysis on the *ECEL1* mutation outcome on protein function, our results are consistent with prior studies and further support a role for *ECEL1* in the development of the neuromuscular junction of human skeletal muscles of both the limbs and the trunk (Dieterich et al., 2013; Shaheen et al., 2014).

To better understand the role of *ECEL1* in human clinical research, experimental researches have been done to find the etiology as well as the genotype–phenotype relationships of *ECEL1* mutations. Based on previously reported abnormal phenotypes of DA hind limb in two siblings, Nagata et al., developed a new knock-in mouse carrying an ECEL1/DINE pathogenic G607S missense variant. They have compared the morphological phenotypes of G607S knock-in mice with C760R knock-in mice that formerly established. The similar axonal arborization defects with normal trajectory patterns from the spinal cord to the target hind limb muscles and with also axon guidance defects of the abducens nerves were seen in both of the knock-in mouse embryos (C760R and G607S). These findings showed that the ECEL1/DINE variants causes motor innervation defects as primary reasons in *ECEL1*-mutated congenital contracture disorders (Nagata et al., 2017). The aggregation, inefficacity, and decrease of metal-binding affinity were evaluated due to the effect of point mutation K179E in the *ECEL1* gene by the dynamic analysis first of all we used the best online prediction tools to predict the damaging effect of K179E mutation on ECEL1 protein function. Thereafter, concerning RMSD, RMSF, Rg, and PCA, considerable structural differences between wild-type and mutant *ECEL1* were showed in MD simulation moreover, in the analysis of secondary structure is indicated that the discrepancy in the structural digression, protein motion and increase in the beta-strand content by manifesting he cause for inefficiency and aggregation in the mutant *ECEL1*. In addition, the reason for the lack of the Zn ion binding in mutation in the ECEL1 protein has been identified by average atomic distance and SMD analysis among the wild-type and mutant.

Overall, in this study, we present knowledge of the effect of the studied variant on the ECEL1 protein leading to neurodegenerative disorder in humans. This work may hopefully be supplementary to classical molecular dynamics to dissolve the mutational effects of cofactor-dependent protein.

CONFLICT OF INTEREST STATEMENT
The authors declare that they have no competing interests.

AUTHOR CONTRIBUTONS
Study conception and design: Najmeh Ahangari, Majid Ghayour Mobarhan, Ehsan Ghayoor Karimiani, and Ali Akbar Haddad-Mashhadrizeh. Data collection: Najmeh Ahangari, Mohammad Doosti, and Sima Shahrokhzadeh.

REFERENCES

Colovos, C., & Yeates, T. (1993). Verification of protein structures: Patterns of nonbonded atomic interactions. *Protein Science*, *2*(9), 1511–1519.

Dieterich, K., Quijano-Roy, S., Monnier, N., Zhou, J., Fauré, J., Smirnow, D. A., Carlier, R., Laroche, C., Marcorelles, P., Mercier, S., Mégarbané, A., Odent, S., Romero, N., Sternberg, D., Marty, I., Estournet, B., Jouk, P. S., Melki, J., & Lunardi, J. (2013). The neuronal endopeptidase ECEL1 is associated with a distinct form of recessive distal arthrogryposis. *Human Molecular Genetics*, *22*(8), 1483–1492.

Eisenberg, D., Lüthy, R., & Bowie, J. U. (1997). [20] VERIFY3D: assessment of protein models with three-dimensional profiles. In *Methods in enzymology* (Vol. 277, pp. 396–404). Elsevier.

Gholampour-Faroji, N., Farazmand, R., Hemmat, J., & Haddad-Mashadrizeh, A. (2019). Modeling, stability and the activity assessment of glutathione reductase from streptococcus thermophilus; insights from the in-silico simulation study. *Computational Biology and Chemistry*, 107121.

Hess, B., Bekker, H., Berendsen, H. J., & Fraaije, J. G. (1997). LINCS: A linear constraint solver for molecular simulations. *Journal of Computational Chemistry*, *18*(12), 1463–1472.

Laskowski, R. A., Macarthur, M. W., Moss, D. S., & Thornton, J. M. (1993). PROCHECK: A program to check the stereochemical quality of protein structures. *Journal of Applied Crystallography*, *26*(2), 283–291.

Li, X., Zhong, B., Han, W., Zhao, N., Liu, W., Sui, Y., Wang, Y., Lu, Y., Wang, H., Li, J., & Jiang, M. (2015). Two novel mutations in myosin binding protein C slow causing distal arthrogryposis type 2 in two large Han Chinese families may suggest important functional role of immunoglobulin domain C2. *PLoS One*, *10*(2), e0117158.

Nagata, K., Takahashi, M., Kiryu-Seo, S., Kiyama, H., & Saido, T. C. (2017). Distinct functional consequences of ECEL1/DINE missense mutations in the pathogenesis of congenital contracture disorders. *Acta Neuropathologica Communications*, *5*(1), 1–14.

Patil, S. J., Rai, G. K., Bhat, V., Ramesh, V. A., Nagarajaram, H., Matalia, J., & Phadke, S. R. (2014). Distal arthrogryposis type 5D with a novel ECEL1 gene mutation. *American Journal of Medical Genetics Part A*, *164*(11), 2857–2862.

Pires, D. E., Chen, J., Blundell, T. L., & Ascher, D. B. (2016). In silico functional dissection of saturation mutagenesis: Interpreting the relationship between phenotypes and changes in protein stability, interactions and activity. *Scientific Reports*, *6*, 19848.

Shaheen, R., Al-Owain, M., Khan, A., Zaki, M., Hossni, H., Al-Tassan, R., Eyaid, W., & Alkuraya, F. S. (2014). Identification of three novel ECEL1 mutations in three families with distal arthrogryposis type 5D. *Clinical Genetics*, *85*(6), 568–572.

Shirotani, K., Tsubuki, S., Iwata, N., Takaki, Y., Harigaya, W., Maruyama, K., Kiryu-Seo, S., Kiyama, H., Iwata, H., Tomita, T., Iwatsubo, T., & Saido, T. C. (2001). Neprilysin degrades both amyloid β peptides 1–40 and 1–42 most rapidly and efficiently among thiorphan-and phosphoramidon-sensitive endopeptidases. *Journal of Biological Chemistry*, *276*(24), 21895–21901.

Valdenaire, O., Rohrbacher, E., Langeveld, A., Schweizer, A., & Meijers, C. (2000). Organization and chromosomal localization of the human ECEL1 (XCE) gene encoding a zinc metallopeptidase involved in the nervous control of respiration. *Biochemical Journal*, *346*(3), 611–616.

Whyte, T., Cirak, S., Oprea, I., Beales, P., Osborn, D., Busch, K., Hurles, M., Longman, C., Quinlivan, R., Sewry, C., & Jungbluth, H. (2014). GP 154: Mutations in ECEL1 lead to distal arthrogryposis type 5D. *Neuromuscular Disorders*, *24*(9), 847–848.